

COBE Constraints on a Compact Toroidal Low-density Universe

Kaiki Taro Inoue

Yukawa Institute for Theoretical Physics, Kyoto University, Kyoto 606-8502, Japan

(October 29, 2018)

Abstract

In this paper, the cosmic microwave background (CMB) anisotropy in a multiply-connected compact flat 3-torus model with the cosmological constant is investigated. Using the COBE-DMR 4-year data, a full Bayesian analysis revealed that the constraint on the topology of the flat 3-torus model with low-matter-density is less stringent. As in compact hyperbolic models, the large-angle temperature fluctuations can be produced as the gravitational potential decays at the Λ -dominant epoch well after the last scattering. The maximum allowed number N of images of the cell (fundamental domain) within the observable region at present is approximately 49 for $\Omega_m = 0.1$ and $\Omega_\Lambda = 0.9$ whereas $N \sim 8$ for $\Omega_m = 1.0$ and $\Omega_\Lambda = 0$.

98.70.Vc,98.80.Hw

arXiv:astro-ph/0011462v2 30 Apr 2001

I. INTRODUCTION

For a long time, cosmologists have assumed the simply connectivity of the spatial hypersurface of the universe. If it is the case, the topology of closed 3-spaces is limited to that of a 3-sphere if Poincaré's conjecture is correct. However, if we assume that the spatial hypersurface is multiply connected, then the geometry of spatially finite models can be flat or hyperbolic as well. The metric describes only the local geometry. We should be able to observe the imprint of the "finiteness" of the spatial geometry if it is multiply connected on scales of the order of the particle horizon or less, in other words, if we live in a "small universe".

For flat multiply connected models without the cosmological constant, various constraints using the COBE DMR data have been obtained [1–7]. Assuming that the initial power spectrum is scale-invariant ($n=1$) the suppression of the temperature fluctuations on scales beyond the typical size of the cell L^1 leads to a decrease in the large-angle power. For 3-torus models without the cosmological constant in which the cell (fundamental domain) is a cube, the constraint is $L > 0.8R_*$ where R_* is the comoving radius of the last scattering surface(horizon radius) [1–4]. It should be emphasised that the constraint itself *does not imply that the "small universe" is ruled out* since the possible maximum expected number of the copies of the cell within the observable region at present is approximately 8. For models in which one side of the cell is longer than the others, the constraint for the smallest topological identification scale(=the diameter of the smallest ball which can wrap around the space) can be less stringent [7].

On the other hand, recent observations of distant supernova Ia [8,9] imply the existence of "missing energy" which possesses a negative pressure and equation-of-state ($w \equiv p/\rho$) in the form of either a cosmological constant, vacuum energy density or a slowly-varying spatially inhomogeneous component "quintessence". Together with the first observation of the height and the position of the first Doppler peak by BOOMERANG [10] and MAXIMA [11] and the COBE-DMR data, the constraint for the cosmological constant is $0.69 < \Omega_\Lambda < 0.82$ and for the matter(cold dark matter, baryon plus radiation) $0.28 < \Omega_m < 0.42$ assuming adiabatic initial perturbations [12].

For low-matter-density models with flat geometry a bulk of large-angle cosmic microwave background(CMB) fluctuations can be produced as the gravitational potential decays at the Λ -dominant epoch $1+z \sim (\Omega_\Lambda/\Omega_0)^{1/3}$. Recent works [13–16] have shown that the angular power spectrum C_l is completely consistent with the COBE-DMR data for some compact hyperbolic models which are incompatible with the previous analyses [17]. Because the angular sizes of fluctuations produced at the late epoch are large compared to those on the last scattering for flat or hyperbolic geometry, we expect that the constraints for compact flat models with low-matter-density can be also significantly loosened.

In this paper, the CMB anisotropy in a multiply-connected compact flat 3-torus model with or without the cosmological constant is investigated. In sec II we briefly describe the time evolution of the scalar perturbation in the locally flat Friedmann-Robertson-Walker

¹ L can be defined as twice the diameter which is defined as the maximum of the minimum geodesic distance between two points over the space.

models which will be used for computing the CMB anisotropy. In sec III we compare the angular power spectrum in a flat 3-torus model with the cosmological constant to the one in the “standard” 3-torus model with $\Omega_{tot}=1$. In sec IV a full Bayesian analysis using the COBE-DMR data has been carried out for giving the constraint on the minimum size of the cell.

II. CMB ANISOTROPY

In what follows we assume that the matter consists of two components: a relativistic one and a non-relativistic one ($\Omega_m = \Omega_r + \Omega_n$). First of all we consider the evolution of the background space. From the Friedmann equation, the integral representation for the time evolution of the scale factor a (normalised to 1 at present time) in terms of the conformal time η takes the form

$$\eta(a) = H_0^{-1} \int_0^a \frac{da}{\sqrt{\Omega_{n0}a + \Omega_{r0} + \Omega_\Lambda a^4}} \quad (1)$$

where H_0 , Ω_{r0} and Ω_{n0} are the Hubble parameter, the density parameter for relativistic and non-relativistic matter at present, respectively. Note that (1) can be written in terms of the elliptic integral of the first kind which is too complex to describe here. The radius of the last scattering surface R_* in comoving coordinates can be obtained by integrating η from $1/(z_{LSS}) \sim 1/1100$ to 1. One can easily see that the presence of Ω_Λ makes R_* to a larger value. For a fixed H_0 and the total density at present Ω_{tot} , the presence of a cosmological constant or vacuum energy implies a decrease in the cosmological expansion rate in earlier epoch which augments the age of the universe and the size of the causally connected region. As for the radiation density, the standard scenario of the thermal history gives the present density $\Omega_{r0} = \Omega(\text{photon}) + \Omega(\text{neutrino}) = 4.15 \times 10^{-5} h^{-2}$ assuming three generations for neutrinos [18]. Applying the value to (1) one obtains $R_* = 4.98$ for $(\Omega_{n0}, \Omega_\Lambda) = (0.1, 0.9)$ while $R_* = 1.99$ for $(\Omega_{n0}, \Omega_\Lambda) = (1.0, 0)$.

Next, we consider the time evolution of the scalar-type perturbation. Assuming that the anisotropic pressure is negligible, in the Newtonian gauge, the Newtonian curvature perturbation Φ in k space satisfies [19],

$$\Phi'' + 3\mathcal{H}(1 + c_s^2)\Phi' + c_s^2 k^2 \Phi + (2\mathcal{H}' + (1 + 3c_s^2)\mathcal{H}^2)\Phi = -4\pi G a^2 p \Gamma, \quad (2)$$

$$c_s^2 = \frac{1}{3} \frac{\rho_r}{\rho_n + \frac{3}{4}\rho_r},$$

$$\Gamma = \frac{\rho_n}{\rho_r + \frac{3}{4}\rho_n} \left(\frac{3}{4} \frac{\delta\rho_r}{\rho_r} - \frac{\delta\rho_n}{\rho_n} \right), \quad (3)$$

where ' denotes the conformal time derivative $d/d\eta$, $\mathcal{H} \equiv a'/a$, G is the Newton's constant, p is the total pressure, c_s is the sound speed of the fluid and Γ corresponds to the entropy perturbation defined as $p\Gamma \equiv \delta p - \frac{p'}{\rho'} \delta\rho$. Assuming a pure adiabatic perturbation ($\Gamma = 0$), the amplitudes of Φ for the non-decaying mode are constant in the radiation dominant

epoch if $k\eta_{eq} \ll 1$ [19]. Hence the non-decaying mode of the perturbation that enters the Hubble radius after the radiation-matter equality time η_{eq} can be obtained by setting the initial condition $\Phi'(0) = 0$. In practice, we approximate the solution of (1) by interpolating polynomial functions which are used for numerically solving the second order ordinary differential equation (2).

For superhorizon perturbations, the amplitudes of Φ are constant in the radiation dominant epoch ($\Phi/\Phi(0) = 1$) and in the matter dominant epoch ($\Phi/\Phi(0) = 9/10$) However, in the Λ -dominant epoch Φ gradually decays as $1/a$ that will play a critical role in characterising the large-angle temperature fluctuations for Λ -models.

Assuming a pure adiabatic initial condition and neglecting the anisotropic pressure, the temperature fluctuation on large angular scales can be written in terms of the curvature perturbation Φ as

$$\frac{\Delta T}{T}(\mathbf{n}) = -\frac{1}{3}\Phi(\eta_*, (\eta_0 - \eta_*)\mathbf{n}) - 2 \int_{\eta_*}^{\eta_0} \frac{\partial\Phi(\eta, (\eta_0 - \eta)\mathbf{n})}{\partial\eta} d\eta, \quad (4)$$

where \mathbf{n} denotes the unit vector which points towards the sky and η_* and η_0 correspond to the last scattering and the present conformal time, respectively [20,21]. The first term in the right-hand side in (4) describes the ordinary Sachs-Wolfe (OSW) effect while the second term describes the integrated Sachs-Wolfe (ISW) effect. Note that the Sachs-Wolfe formula (4) is valid only for perturbations whose scale is sufficiently larger than the horizon radius at the last scattering $k < 1/\eta_*$. From (1), one obtains the conditions $k < 20.5H_0$ for $(\Omega_m, \Omega_\Lambda) = (1.0, 0)$ and $k < 9.9H_0$ for $(\Omega_m, \Omega_\Lambda) = (0.1, 0.9)$. The effect of the acoustic oscillations becomes important for fluctuations on smaller scales. However, for large angular scales ($l < 15$), contributions from acoustic oscillations are negligible.

III. POWER SPECTRUM

Let us now consider cosmological models whose spatial geometry is represented by a flat 3-torus which is obtained by gluing the opposite faces of a cube by three translations. Then the wave numbers of the square-integrable eigenmodes of the Laplacian are restricted to the discrete values $k_i = 2\pi n_i/L$, ($i = 1, 2, 3$) where n_i 's run over all integers. The angular power spectrum is written as

$$C_l = \sum_{\mathbf{k} \neq 0} \frac{8\pi^3 \mathcal{P}_\Phi(k) F_{kl}^2}{k^3 L^3},$$

$$F_{kl} = \frac{1}{3}\Phi(\eta_*) j_l(k(\eta_0 - \eta_*)) + 2 \int_{\eta_*}^{\eta_0} \frac{d\Phi}{d\eta} j_l(k(\eta_0 - \eta)), \quad (5)$$

where $\mathcal{P}_\Phi(k)$ is the initial power spectrum for Φ and $k \equiv \sqrt{k_1^2 + k_2^2 + k_3^2}$. From now on we assume the scale-invariant Harrison-Zeldovich spectrum ($\mathcal{P}_\Phi(k) = const.$) as the initial power spectrum.

FIGURES

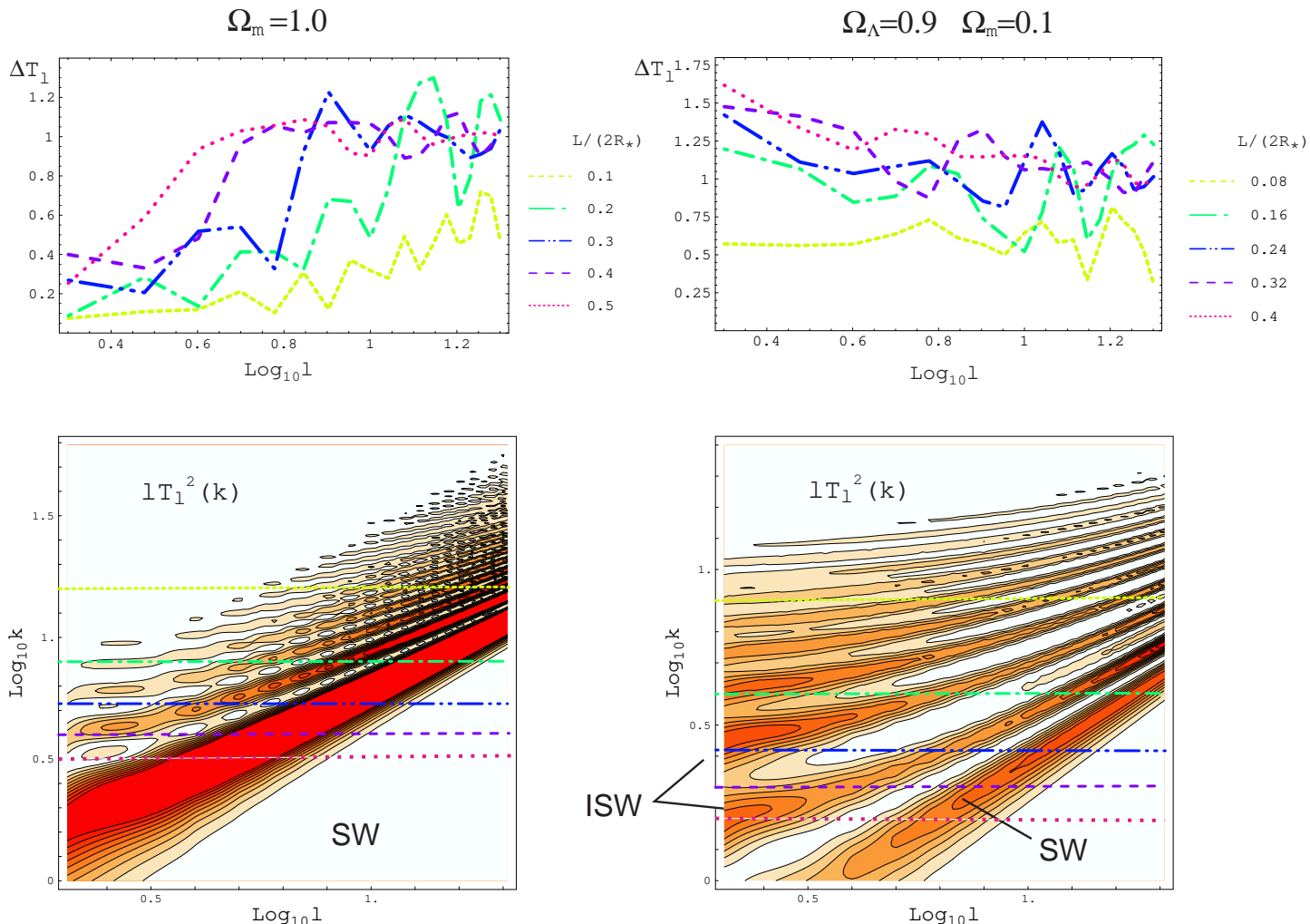


FIG. 1. Suppression in large-angle power for 3-torus models with or without the cosmological constant. A large-angle suppression in $\Delta T_l \equiv \sqrt{l(l+1)C_l/(2\pi)}$ (all the plotted values are normalised by ΔT_{20} with infinite volume) occurs for the “standard” 3-torus model $(\Omega_m, \Omega_\Lambda) = (1.0, 0)$ at $l < l_{cut} \sim 2\pi R_*/L - 1$ while such a prominent suppression is *not* observed for the 3-torus model with $(\Omega_m, \Omega_\Lambda) = (0.1, 0.9)$. The transfer function $T_l(k)$ describes how each k -mode contributes to the power for a particular angular scale l . The corresponding first eigenvalues k_1 are plotted as horizontal lines (lower figures). The unit of k is H_0 .

Now let us estimate the angular scale below which the power spectrum is suppressed owing to the mode-cutoff $k_{cut} = 2\pi/L$. First of all we consider the transfer function $T_l(k)$ which is defined by

$$\frac{2l+1}{4\pi}C_l = \int T_l^2(k)\mathcal{P}(k)\frac{dk}{k}, \quad (6)$$

that describes how the spatial information is included in the angular power. For a given k , the contribution to the angular power on smallest angular scales comes from the OSW

effect where the transfer function can be written in terms of the spherical Bessel function as $T_l^{OSW}(k) = j_l(k\eta_0)$. Because $j_l(x)$'s have the first peaks at $x \sim 1 + l$, the angular cutoff l_{cut} is determined by $l_{cut} = 2\pi\eta_0/L - 1$. For instance, $l_{cut} \sim 5$ for $L = \eta_0 = 2H_0^{-1}$. Thus the large-angle suppression scale is determined by the largest fluctuation scale at the last scattering. On smaller angular scales $l > l_{cut}$, the second peak in the power corresponds to the fluctuation scale of the second eigenmode at the last scattering. This behavior is analogous to the acoustic oscillation where the oscillation scale is determined by the sound horizon at the last scattering. On angular scales larger than l_{cut} one observes another oscillation feature in the power for models with a smaller cell where $k_{cut}\eta_0$ is sufficiently large which is apparently determined by the behavior of the first eigenmode. From the asymptotic form

$$j_l(x) \sim \frac{1}{x} \sin(x - l\pi/2), \quad x \gg \frac{l(l+1)}{2}, \quad (7)$$

one notices that the angular scale of the oscillation for asymptotic values $k_{cut}\eta_0 \gg l(l+1)/2$ is $\Delta l = 2$. For intermediate values of $k_{cut}\eta_0$, Δl take much larger values (see figure 1).

So far, we have studied the effect of the non-trivial topology on the OSW contribution only which is sufficient for constraining the topology of the ‘‘standard’’ 3-torus model with $\Omega_{tot} = 1$. However, for low-matter-density models, one cannot ignore the (late) ISW contribution which is generated by the decay of the gravitational potential at the Λ -dominant epoch. The crucial point is that they are produced at *later* time $1 + z \sim (\Omega_\Lambda/\Omega_0)^{1/3}$ well after the last scattering. Although it is impossible to generate fluctuations beyond the size of the cell (in 3-dimensional sense), that does not necessarily mean that any fluctuations on large angular scales (in 2-dimensional sense) cannot be produced. Suppose that a fluctuation is produced at a point nearer to us, then the corresponding angular scale becomes large if the background geometry is flat or hyperbolic. Therefore, one can expect that the suppression on large angular scales owing to the mode-cutoff is not stringent for low-matter-density models. As shown in figure 1, the angular powers for a model with $(\Omega_\Lambda, \Omega_m) = (0.9, 0.1)$ are almost flat. In contrast to the ‘‘standard’’ model, the transfer function for low-matter-density models distributes in a broad range of k that implies the additional late production of the fluctuations which contribute to the angular power. Surprisingly, in the low-matter-density models with small volume, the slight excess power due to the ISW effect is cancelled out by the moderate suppression owing to the mode-cutoff which leads to a flat spectrum. However, as observed in the ‘‘standard’’ 3-torus model, the power spectra have prominent oscillating features. The oscillation scale for $l < l_{cut}$ is determined by the first eigenmode. The peaks in the angular power correspond to the first SW ridge and the first and the second and other ISW ridges. Is such an oscillating feature already ruled out by the current observation? We will see the results of our Bayesian analyses for testing the goodness-of-fit to the COBE data in the next section.

IV. BAYESIAN ANALYSIS

In general, the covariance in the temperature at pixel i and pixel j in the sky map can be written as

$$M_{ij} = \langle T_i T_j \rangle = \sum_l \langle a_{lm} a_{l'm'} \rangle W_l W_{l'} Y_{lm}(\hat{n}_i) Y_{l'm'}(\hat{n}_j) + \langle N_i N_j \rangle \quad (8)$$

where a_{lm} is an expansion coefficient with respect to a spherical harmonic Y_{lm} , $\langle \rangle$ denotes an ensemble average taken over all initial conditions, positions and orientations of the observer, T_i represents the temperature at pixel i , W_l^2 is the experimental window function that includes the effect of beam-smoothing and finite pixel size, \hat{n}_i denotes the unit vector towards the center of pixel i and $\langle N_i N_j \rangle$ represents the noise covariance between pixel i and pixel j . If the temperature fluctuations form a homogeneous and isotropic random Gaussian field then the covariance matrix can be written in terms of the power spectrum C_l as

$$M_{ij} = \frac{1}{4\pi} \sum_l (2l+1) W_l^2 C_l P_l(\hat{n}_i \cdot \hat{n}_j) + \langle N_i N_j \rangle \quad (9)$$

where P_l is the Legendre function. Then the probability distribution function of the pixel temperature \vec{T} for the Gaussian field is

$$f(\vec{T}|C_l) = \frac{1}{(2\pi)^{N/2} \det^{1/2} M(C_l)} \exp\left(\frac{1}{2} \vec{T}^T \cdot M^{-1}(C_l) \cdot \vec{T}\right), \quad (10)$$

where N is the number of pixels. Bayes's theorem states that the probability distribution function of a set of parameters \vec{A} given the data \vec{T} is

$$f(\vec{A}|\vec{T}) \propto f(\vec{T}|\vec{A}) f(\vec{A}). \quad (11)$$

If we assume a uniform prior distribution, *i.e.* taking $f(\vec{A})$ to be constant, the probability distribution function of a power spectrum C_l is then

$$\Lambda(C_l|\vec{T}) \propto \frac{1}{\det^{1/2} M(C_l)} \exp\left(\frac{1}{2} \vec{T}^T \cdot M^{-1}(C_l) \cdot \vec{T}\right). \quad (12)$$

Before applying the method to the flat 3-torus models one must be aware that a flat 3-torus we are considering is globally anisotropic although it is globally homogeneous. In contrast to the standard infinite models, the fluctuations form an anisotropic Gaussian field for a fixed orientation if the initial fluctuation is Gaussian. In other words, for a given l , a set of a_{lm} 's ($-l \leq m \leq l$) are not $2l+1$ independent random numbers. In order to see this, we write a plane wave in terms of eigenmodes in the spherical coordinates,

$$e^{i\mathbf{k}\cdot\mathbf{x}} = \sum_{lm} b_{klm} j_l(kx) Y_{lm}(\mathbf{n}), \quad b_{klm} = 4\pi(i)^l Y_{lm}^*(\hat{\mathbf{k}}), \quad (13)$$

where $\hat{\mathbf{k}}$ denotes the unit vector in the direction of \mathbf{k} . Then we have

$$a_{lm} = \sum_{\mathbf{k}} \Phi(k) b_{klm} F_{kl} \quad (14)$$

where F_{kl} is given by (5). Because a_{lm} is linear in $\Phi(k)$, it is Gaussian. However, they are not independent since b_{klm} 's are proportional to spherical harmonics. The statistical isotropy is recovered iff the size L of the cube becomes infinite where $\hat{\mathbf{k}}$ takes the whole values for

a given k . If one marginalises the likelihood with respect to the $SO(3)$ transformation, or equivalently, the orientation of the observer, the distribution function of a_{lm} becomes non-Gaussian since a_{lm} is written in terms of a sum of a product of a Gaussian variable times a variable that is determined by a spherical harmonic $Y_{lm}(\hat{\mathbf{k}})$ where $\hat{\mathbf{k}}$ is a random variable which obeys a uniform distribution. Thus in principle, in order to compare a whole set of fluctuation patterns over the isotropic ensemble one should use the likelihood function which is different from the Gaussian one.

Nevertheless, we first carry out a Bayesian analysis using the Gaussian likelihood function (12) which depends only on C_l 's (which is $SO(3)$ invariant) in order to estimate the effect of the mode-cutoff imposed by the periodic boundary conditions. In the following analysis, we use the inverse-noise-variance-weighted average map of the 53A,53B,90A and 90B COBE-DMR channels. To remove the emission from the galactic plane, we use the extended galactic cut (in galactic coordinates) [22]. After the galactic cut, best-fit monopole and dipole are removed using the least-square method. To achieve efficient analysis in computation, we compress the data at “resolution 6” $(2.6^\circ)^2$ pixels into one at “resolution 5” $(5.2^\circ)^2$ pixels for which there are 1536 pixels in the celestial sphere and 924 pixels surviving the extended galactic cut. The window function is given by $W_l = G_l F_l$ where F_l are the Legendre coefficients for the DMR beam pattern [23] and G_l are the Legendre coefficients for a circular top-hat function with area equal to the pixel area which account for the pixel smoothing effect (which is necessary for “resolution 5” pixels since the COBE-DMR beam FWHM is comparable to the pixel size) [24]. To account for the fact that we do not have useful information about monopole and dipole anisotropy, the likelihood must be integrated over C_0 and C_1 in principle. However, in practice we set $C_0 = C_1 = 100mK^2$ which renders the likelihood insensitive to monopole and dipole moments of several mK . We also assume that the noise in the pixels is uncorrelated from pixel to pixel which is found to be a good approximation [25].

From figure 2 one can see that the constraint on the size of the cell is less stringent for the low-matter-density model as expected from the shape of the power spectrum. The effect of the suppression of the large-angle power is not prominent unless the cell size is sufficiently smaller than the observable region ($L < 0.8H_o^{-1} = 0.08 \times 2R_*$ for $\Omega_m = 0.1$). However, the likelihood function varies rapidly as the size increases since the power is jagged in l . Unfortunately, the peaks in the power at $l \sim 6$ and $l \sim 11$ which correspond to the first and the second ISW ridge give a bad fit to the COBE data for $L \sim 1.7H_o = 0.17 \times 2R_*$. However, the parameter range which gives a good fit to the data is wider for the low-matter-density model. It should be emphasised that for both flat models there is a parameter region in which the fit is much better than the infinite counterpart. For example, the peaks at $l \sim 4$ and $l \sim 9$ in the angular power of the low-matter-density model with $L \sim 2.8H_o^{-1}$ give a much better fit to the COBE data than the infinite counterpart. In fact the quadrupole component in the COBE data is very low and the angular power is peaked at $l \sim 4$. For infinite flat Λ -models with a scale-invariant initial spectrum such features can be a problem since the ISW contribution gives an excess power on large angular scales.

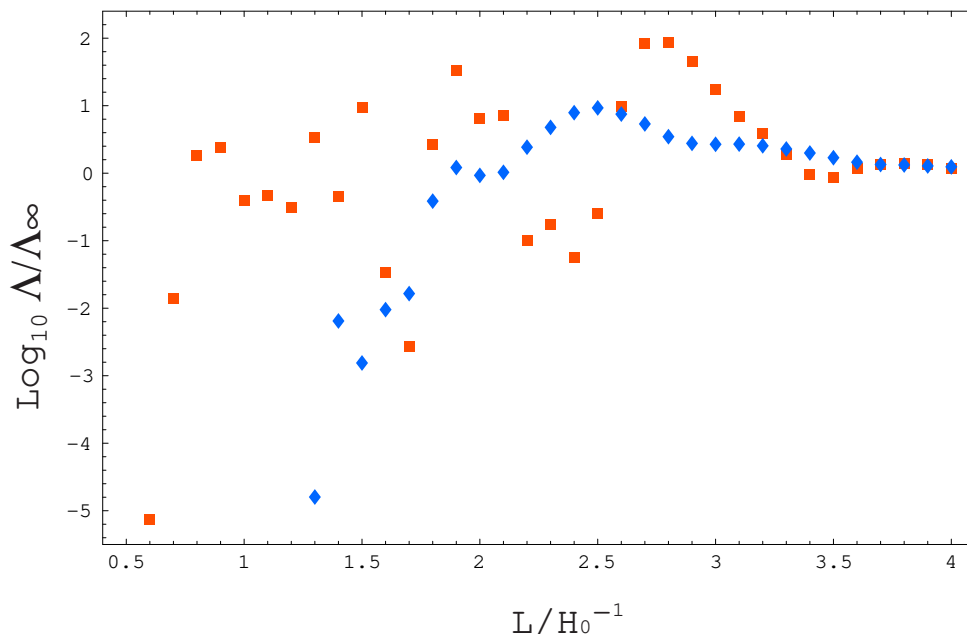


FIG. 2. The likelihoods of the 3-torus models with $(\Omega_m, \Omega_\Lambda) = (1.0, 0)$ (diamond) and $(0.1, 0.9)$ (box) relative to the infinite models with the same density parameters are plotted. The likelihoods are marginalised over the quadrupole normalisation $Q \equiv (5C_2/(4\pi))^{1/2}$. An isotropic Gaussian approximation has been used for computing the likelihoods. The COBE-DMR data is compressed to 924 pixels at “resolution 5”.

Next, we carry out a full Bayesian analysis in which all the elements of $\langle a_{lm}a_{l'm'} \rangle$ are included. Because of the limit in the CPU power we further compress the data at “resolution 5” pixels to “resolution 3” $(20.4^\circ)^2$ pixels in galactic coordinates for which there are 60 pixels surviving the extended galactic cut. Although the information on smaller angular scales $l > 10$ is lost, we expect that they still provide us a sufficient information for discriminating the effect of the non-trivial topology since it is manifest on large angular scales. The computation has been done in a similar manner as previous analysis except for the covariance matrix for which we use (8) instead of (9). The likelihoods Λ are computed for a total of 2000 random orientations for each model using a vector parallel supercomputer vpp 800. The approximated likelihoods which depend on only the power spectra are also computed for comparison.

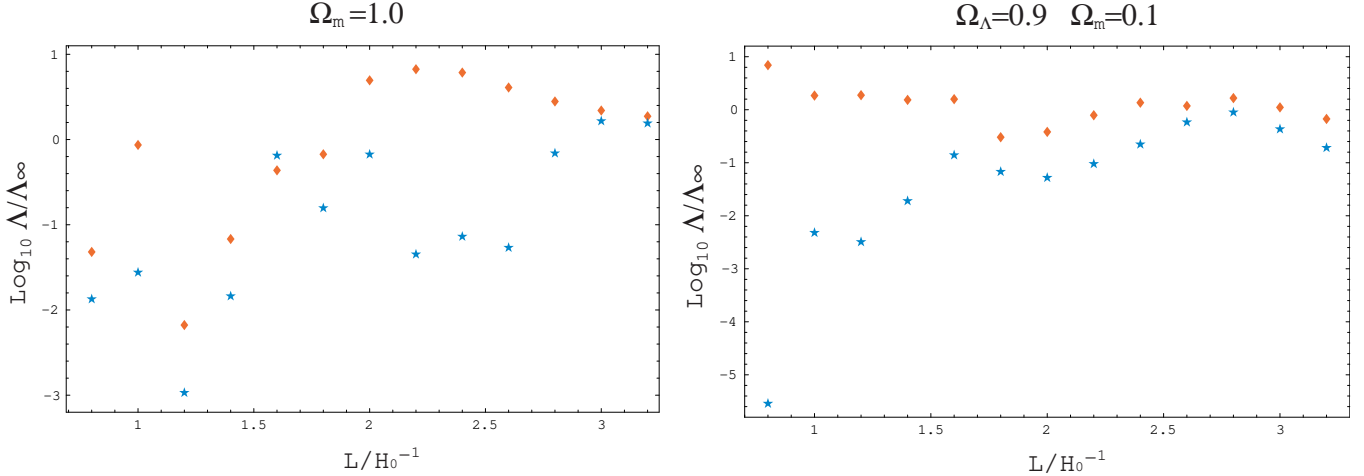


FIG. 3. The likelihoods of the 3-torus models relative to the infinite models with the same density parameters marginalised over 2000 orientations (star) and that using only the power spectrum (diamond). The inverse-noise-variance-weighted average map of the COBE-DMR data is compressed to 60 pixels (resolution 3). All the likelihoods are also marginalised over the quadrupole normalisation $Q \equiv (5C_2/(4\pi))^{1/2}$.

As shown in figure 3, the discrepancy between the likelihood marginalised over the orientation of the observer and the approximated likelihood is prominent for models with small volume in which the effect of the non-trivial topology is significant. Let us estimate the size of the cell for which the effect becomes insignificant. For the “standard” model with $\Omega_m = 1.0$, the volume of the observable region is $4\pi R_*^3/3 \sim 34$ which gives the critical scale $L_c \sim 3.2H_0^{-1}$ for which the volume of the cell is comparable to the volume of the observable region at present. For the low-matter-density model a significant amount of large-angle fluctuations are produced at the Λ -dominant epoch $z \sim 1$. Therefore one should compare the volume of the sphere with radius $\eta(z=0) - \eta(z=1) \sim 0.9H_0^{-1}$ to the volume of the cell instead of the observable region which gives $L_c \sim 1.5H_0^{-1}$. We can see from figure 3 that these estimates well agree with the numerical result.

We can give two explanations for the discrepancy although they are related each other. One is the non-Gaussianity in the fluctuations and another one is the correlations between a_{lm} 's owing to the global anisotropy in the background geometry.

Suppose a random variable $Z = XY$ in which X obeys a distribution function $E(X)$ which is even and Y obeys a distribution function $F(Y)$. Then the distribution function G of Z is given by

$$G(Z) = \int \frac{E(Z/Y)}{|Y|} F(Y) dY, \quad (15)$$

which is apparently even. Because the fluctuations are written in terms of a sum of products of Gaussian variable $\Phi(k)$ (with zero average) times a non-Gaussian variable $Y_{lm}(\hat{\mathbf{k}})$, the skewness in the distribution function of a_{lm} marginalised over the orientation is zero although the kurtosis is non-zero.

The correlations in a_{lm} 's are the consequence of the gap between the degree of freedom

of $(\hat{\mathbf{k}})$ and (l, m) . The degeneracy number in a k -mode (=the number of the direction $\hat{\mathbf{k}}$) is much less than the number of relevant “quantum numbers” $(l, m)^2$ if the scale ($=2\pi/k$) is comparable to the length of the side L . Taking an ensemble average over the initial condition we have

$$\langle a_{lm}a_{l'm'} \rangle = \sum_{\mathbf{k} \neq 0} \frac{8\pi^3}{k^3 L^3} \mathcal{P}_\Phi(k) Y_{lm}(\hat{\mathbf{k}}) Y_{l'm'}(\hat{\mathbf{k}}) F_{kl} F_{kl'}, \quad (16)$$

where F_{kl} is given by (5). The sum does not vanish in general when $(l, m) \neq (l', m')$ which is the consequence of the global anisotropy in the background geometry. However, if one takes an average of (16) over $\hat{\mathbf{k}}$, one finds that all off-diagonal elements vanish because of the orthogonality of the spherical harmonics. Similarly one can consider 4-point correlations $\langle a_{l_1 m_1} a_{l_2 m_2} a_{l_3 m_3} a_{l_4 m_4} \rangle$. In this case, all the off-diagonal elements $(l_i, m_i) \neq (l_j, m_j)$ do not necessarily vanish even if one takes an average over $\hat{\mathbf{k}}$. Thus the non-Gaussianity for the flat 3-torus models contrasts sharply with the one for the compact hyperbolic models in which the pseudo-random Gaussian property of the expansion coefficients b_{klm} (which are obtained by expanding the eigenmode in terms of eigenmodes in the universal covering space) [26,27] renders off-diagonal elements always vanish if an average is taken over the position of the observer(although the kurtosis is non-zero). The difference can be attributed to the property of eigenmodes. In a less rigorous manner the property of the eigenmodes which are projected onto a sphere with large radius can be stated as follows: *Projected eigenmodes of compact hyperbolic spaces are “chaotic” whereas those of compact flat spaces are “regular”*.

As for the constraint on the size of the cell, we set a slightly severe condition for the low-matter-density model since the likelihood of the infinite counterpart is $\sim 10^{-1}$ of that of the infinite “standard” model due to a slight boost on the large angular scales caused by the ISW effect. Together with the previous analysis using the data on the “resolution 5” pixels, the conditions on the relative likelihood $\log_{10}(\Lambda/\Lambda_\infty) > -2$ and $\log_{10}(\Lambda/\Lambda_\infty) > -1$ yield $L \geq 1.6H_0^{-1}$ and $L \geq 2.2H_0^{-1}$ for the “standard” 3-torus model $(\Omega_m, \Omega_\Lambda) = (1.0, 0)$ and the low-matter-density 3-torus model $(\Omega_m, \Omega_\Lambda) = (0.1, 0.9)$, respectively. Here Λ_∞ denotes the likelihood of the infinite counterpart with the same density parameters. The maximum number N of images of the cell within the observable region at present is 8 and 49 for the former and the latter, respectively. Note that the constraint on the “standard” 3-torus model is consistent with the previous result [3,4].

²Here we assumed that for each degenerated mode specified by $\hat{\mathbf{k}}$, $\Phi(k)$ are independent Gaussian variables.

V. SUMMARY

In this paper the CMB anisotropy in a flat 3-torus model with or without the cosmological constant has been investigated. Using the COBE-DMR data, we have done a full Bayesian analysis incorporating the effect of anisotropic correlation. It has turned out that the constraint on the low-matter-density model is less stringent compared to the “standard” model with $\Omega_m = 1.0$. The reason is that the large-angle fluctuations (on COBE scales) are produced at late time well after the last scattering. The physical size of these fluctuations is of the order of the size of the cell or less. Hence the effect of the non-trivial topology becomes insignificant. We expect that the result does not significantly change for other compact flat models with different topology [6] or with different shape of the cell since the physical effect does not change.

We have seen that the analysis using the angular power spectrum is not enough since the background geometry is globally anisotropic. Even if the power spectrum well agrees with the data, it does not guarantee the validity of the model since the power spectrum has information of only isotropic components in the 2-point correlations. If the background geometry is globally anisotropic then the fluctuations form an anisotropic Gaussian field for a given orientation. On the other hand, the fluctuations become non-Gaussian if one marginalises the distribution function over the orientation [28]. For locally Friedmann-Robertson-Walker models which are spatially compact, we expect to observe zero skewness but non-zero kurtosis provided that the initial fluctuation is Gaussian.

However, for low-matter density models, anisotropy in the statistically averaged correlation on large angular scale cannot be so large since the physical size of observed temperature fluctuations that has been produced well after the last scattering is much smaller than the actual size of the space (i.e. topological identification scale).

In the case of flat topology, the discrete eigenmodes have “regular” features which lead to significant correlations in a_{lm} ’s. Even if marginalised over the orientation, the correlations do not completely disappear. This contrasts with the case of hyperbolic topology in which the discrete eigenmodes are “chaotic” and the correlations in a_{lm} ’s disappear if one takes an average over the position of the observer.

In order that we would be able to observe the periodic structure in the fluctuations for the 3-torus models, we need to have $L/(2R_*) < 1$ where R_* is the comoving radius of the last scattering surface. Because the obtained constraints give $L/(2R_*) > 0.40, 0.22$ for $(\Omega_m, \Omega_\Lambda) = (1.0, 0), (0.1, 0.9)$, respectively, we still have a great chance of the first detection of the non-trivial topology of the universe by the future satellite missions such as MAP and *Planck* which can survey the CMB in the full sky with high resolution by measuring some specific signatures (e.g. the circles test [29] or the non-Gaussianity [27]).

ACKNOWLEDGMENTS

I would like to thank N. Sugiyama, T. Chiba for their useful advice and comments and A.J. Bandy for his advice on the use of the COBE data. The numerical computation in this work was carried out at the Data Processing Center in Kyoto University and Yukawa Institute Computer Facility. K.T. Inoue is supported by JSPS Research Fellowships for

Young Scientists, and this work is supported partially by Grant-in-Aid for Scientific Research Fund (No.9809834).

REFERENCES

- [1] Sokolov I Y 1993 *JETP Lett.* **57** 617
- [2] Starobinsky A A 1993 *JETP Lett.* **57** 622
- [3] Stevens D, Scott D and Silk J 1993 *Phys. Rev. Lett.* **71** 20
- [4] de Oliveira-Costa A, Smoot G F 1995 *Astrophys. J.* **448** 447
- [5] de Oliveira-Costa A, Smoot G F and Starobinsky A A 1996 *Astrophys. J.* **468** 457
- [6] Levin J Scannapieco E and Silk J 1998 *Phys. Rev. D* **58** 103516
- [7] Roukema B F 2000 astro-ph/0007140
- [8] Perlmutter S *et al* 1999 *Astrophys. J.* **517** 565
- [9] Riess A *et al* 1999 *Astron. J.* **117** 707
- [10] Melchiorri A *et al* 2000 *Astrophys. J.* **536** Issue 2 L63
- [11] Balbi A *et al* 2000 astro-ph/0005124 accepted in *Astrophys. J. Letters*
- [12] Balbi A *et al* 2000 astro-ph/0011202 to appear in *Proc. Cosmology and Particle Physics of the CAPP 2000 Conference Verbier, Switzerland, July 2000* eds. Garcia-Bellido J, Durrer R and Shaposhnikov M (AIP)
- [13] Aurich R 1999 *Astrophys. J.* **524** 497
- [14] Inoue K T, Tomita K and Sugiyama N 2000 *Mon. Not. R. Astron. Soc.* **314** 4 L21
- [15] Cornish N J and Spergel D N 2000 *Phys. Rev. D* **62** 087304
- [16] Aurich R and Steiner F 2000 astro-ph/0007264
- [17] Bond J R, Pogosyan D and Souradeep T 1998 *Class. Quantum Grav.* **15** 9 2671
- [18] Kolb E W and Turner M S 1994 *The Early Universe* (New York: Perseus)
- [19] Mukhanov V F, Feldman H A and Brandenberger R H 1992 *Phys. Rep.* **215** 203
- [20] Sachs R K and Wolfe A M 1967 *Astrophys. J.* **147** 73
- [21] Hu W, Sugiyama N and Silk J 1997 *Nature* **386** 37
- [22] Banday A J *et al* 1997 *Astrophys. J.* **475** 393
- [23] Lineweaver C H 1994 *et al Astrophys. J.* **436** 452
- [24] Hinshaw G *et al* 1996 *Astrophys. J.* **464** L17
- [25] Tegmark M and Bunn E F 1995 *Astrophys. J.* **455** 1
- [26] Inoue K T 1999 *Class. Quantum Grav.* **16** 3071
- [27] Inoue K T 2000 *Phys. Rev. D* **62** 103001
- [28] Magueijo J 1997 *Phys. Rev. D* **56** 4578
- [29] Cornish N J, Spergel D and Starkman G 1996 *Phys. Rev. Lett.* **77** 215